# $CO_2$ abatement by two-dimensional MXene carbides†

Ángel Morales-García, Adrián Fernández-Fernández, Francesc Viñes* and Francesc Illas

**Two-dimensional transition metal carbides with $M_2C$ formula (M = Ti, Zr, Hf, V, Nb, Ta, Cr, Mo, W) have been recently synthesized and isolated, and are here presented as very promising candidates for carbon dioxide ($CO_2$) capture, storage, and activation. By means of density functional theory investigations including dispersion we show the strong $CO_2$ uptake and activation on $M_2C$, where estimates of adsorption and desorption rates indicate their $CO_2$ adsorption capacity even at low $CO_2$ partial pressures and high temperatures. The $M_2C$ feature noteworthy $CO_2$ load capacities ranging 2.34–8.25 mol $CO_2$/kg, making them practical materials for $CO_2$ abatement.**

The evergrowing carbon dioxide ($CO_2$) concentration in atmosphere is one of the major responsibles of the greenhouse effect, global warming, and ocean acidification.[1] This increase is ascribed mainly to anthropogenic activities connected to the combustion of fossil fuels, which nowadays demand alternative routes to reduce the $CO_2$ emissions.[2] There exist three primary approaches for reducing the amount of $CO_2$ in the atmosphere; (*i*) by acquiring energy efficient and conservation practices[3] which promote the dropping of $CO_2$ emissions; (*ii*) by reducing the carbon-based energy resources[4] using sustainable technologies such as hydrogen, solar and wind powers, and/or geothermal or biomass derived energies; and (*iii*) by $CO_2$ chemical trapping on active solid-substrates following the carbon capture and storage (CCS) derived strategy.[5]

Among these approaches, CCS appears to have a great potential[6-8] and has gained momentum since it is a feasible route to activate and then convert $CO_2$ into valuable chemical products, *e.g.* liquid fuels,[9] under ambient conditions. Here a solid-substrate is required to fix $CO_2$ but, ideally, one would choose one that activates it through charge transfer leading to a bent anionic $CO_2^{\delta-}$ species.[10,11] Such so-called activated $CO_2$ adsorbate is more prone to react when combined with other surface chemicals, *e.g.* $H_2$ for methanol production.[12] This waste-to-product route then not only reduces the $CO_2$ atmospheric content, but generates at the end of the chemical catalytic chain a saleable added-value product.

Several materials have been pointed for $CO_2$ capture/activation including metals,[13] metal oxides,[14] graphene-based materials,[15] zeolites,[16] and metal-organic frameworks (MOFs),[17] to name a few. Transition metal carbides (TMCs)[18] have recently raised much attention as a potential family of materials for $CO_2$ capture, storage, and activation,[19] with side appealing features including low-cost, thermal and physical robustness, and chemical stability.[20] The initial computational investigations were afterwards experimentally confirmed by $CO_2$ conversion at moderate temperatures.[21] Indeed, TMCs $CO_2$ capture and activation is predicted up to elevated temperatures and low $CO_2$ partial pressures.[19]

However, one technologically drawback of TMCs is their modest effectively exposed surface area ranging 20-450 $m^2$ $g^{-1}$.[22] More attractive are the TMCs two-dimensional (2D) derived counterparts, so-called MXenes —M and X stand for an early transition metal and carbon or nitrogen, respectively. More than 25 different MXene 2D materials have been synthesized from precursor MAX phases using hidrogen fluorine,[23] with at least three different stoichiometries: $M_2X$, $M_3X_2$, and $M_4X_3$,[24] although fluorine-free synthetic procedures have been recently implemented.[25] These 2D TMC display high surface areas in the order of 250-1000 $m^2$/g, conductivities comparable to multilayer graphene, and excellent stabilities.[23]

MXenes have been sucessfully used as alkaline-ion based batteries,[26,27] and catalysts for $H_2$ evolution from water.[28] As stated above, motivated by previous results on TMCs (001) surfaces[19] and by the MXenes large surface area, we investigated here the carbide MXenes capabilities for $CO_2$ sequestration. To facilitate a logical comparison to previous results and to circumvent structural-related effects, we restrained our study to $d^2$ (Ti, Zr, Hf), $d^3$ (V, Nb, Ta), and $d^4$ (Cr, Mo, W) MXenes having a 2:1 M:C ratio, exploring interaction through their (0001) exposed surface. Note that the (0001) surface is equivalent to the (111) surface of bulk refractory TMCs materials featuring face-centered cubic (fcc) crystallographic structure and 1:1 M:C ratio, a surface known to be less stable than (001).[29] Therefore, MXene materials allow one easier access to investigate such surfaces, which are thermodynamically disfavoured in their three-dimensional (3D) TMCs counterparts.[19]

The interaction of $CO_2$ with MXenes (0001) surfaces is here tackled by means of first-principles density functioal theory (DFT) based calculations within the generalized gradient approximation (GGA) using the Perdew-Burke-Ernzerhof (PBE) exchange-correlation functional,[30] as implemented in the Vienna *ab initio* simulation package (VASP).[31] Calculations have been carried out also including the D3 dispersion correction (PBE-D3) developed by Grimme.[32] In the following PBE-D3 zero-point energy (ZPE) corrected adsorption energies are discussed. Further computational details are given in the ESI.† For the sake of oncoming clarity, note that favourable adsorption energies, $E_{ads}$, are defined negative, and the more favourable interactions feature lower $E_{ads}$ values.

To explore the $CO_2$ interaction with the selected MXenes, several adsorption sites have been evaluated implicitly considering different $CO_2$ molecular orientations with respect the material´s surface. After relaxation, five particular sites and/or conformations were identified as stable minima in at least one of the explored MXenes. These are labeled following the coordination notation as $\eta^3$-$CO_2$-$\mu^5$-$C_CO_MO_M$, $\eta^2$-$CO_2$-$\mu^3$-$C_CO_B$, $\eta^3$-$CO_2$-$\mu^5$-$C_MO_CO_C$, $\eta^2$-$CO_2$-$\mu^3$-$C_MO_B$, and $\eta^1$-$CO_2$-$\mu^2$-$C_B$, and depicted in Fig. 1, where latter identification part is sufficient for its recognition —further details about notation are found in ESI†. Note that these sites are not always systematically found for all the explored MXene materials, and depend on each MXene (0001) surface (see ESI†). For instance, the $C_CO_B$ site is generally the least favourable conformation and only competitive in $Mo_2C$, see Table 1; however $C_CO_MO_M$ is the most favourable site to adsorb $CO_2$ on several MXenes: $Ti_2C$, $Zr_2C$, $Hf_2C$, $V_2C$, $Nb_2C$, and $W_2C$. Neglecting dispersion terms raises the average $E_{ads}$ by ~0.40 eV in (see Table S1 in ESI†) with no significant structural variations, in accord to previous studies on TMCs (001) surfaces.[19] Note in passing by that the obtained conformational minima are similar to those previously found on structurally resembling $\beta$-$Mo_2C$ (0001) surface[32] and $M_3C_2$ MXenes,[34] although binding differences appear to occur as a function of the M:C ratio.

Further inspection of Table 1 shows remarkably high $E_{ads}$, ranging from -1.13 ($W_2C$) to -3.69 eV ($Ti_2C$). So, carbide $M_2C$ MXenes essentially double the $CO_2$ bond strength compared equivalent values on parent TMC (001) surfaces, ranging from -0.70 (NbC) to -1.65 (HfC) eV.[19] Furthermore, values spread, including the non-$CO_2$ attaching case of $Cr_2C$. Table 1 data shows an $E_{ads}$ decrease (weaker adsorption) when moving along a *d* series, in agreement with the observed $CO_2$ adsorption on TMCs and $M_3C_2$ MXenes.[19,34] Note that, despite this high energy attachment, $CO_2$ molecules remain intact yet bent —angles $\alpha$(OCO) in the 113-135° range, with elongated C-O bonds —distances $\delta$(CO) in the 1.26-1.51 Å interval, see further details in Table S1 of ESI†. At this stage, the high adsorption energies and structural data support MXenes utilization in $CO_2$ capture and activation, evidented by a high charge transfer according to Bader atoms-in-molecules analysis[35] which confirms the formation of highly anionic $CO_2^{\delta-}$ species with $\delta$- Bader values between -0.90 and -2.86 *e*. The unprecendented high-negative adsorbed $CO_2$ species on $Hf_2C$, with $\delta$- above -2 *e*, seems to imply a higher activity, pointing this MXene for $CO_2$ conversion purposes.

**Table 1** Adsorption energies of $CO_2$ on stable sites of carbide MXenes (0001) surfaces as obtained at PBE-D3 level, ZPE-corrected. PBE and further details are given in Table S1 of the ESI.† All values are given in eV.

| | | $C_CO_MO_M$ | $C_B$ | $C_MO_CO_C$ | $C_MO_B$ | $C_CO_B$ |
|---|---|---|---|---|---|---|
| $d^2$ | **$Ti_2C$** | -3.69 | — | -3.47 | — | -2.88 |
| | **$Zr_2C$** | -3.16 | — | -3.03 | — | — |
| | **$Hf_2C$** | -3.36 | — | -3.33 | — | — |
| $d^3$ | **$V_2C$** | -2.41 | -2.05 | -2.36 | -2.31 | — |
| | **$Nb_2C$** | -2.03 | -1.99 | -2.01 | -2.11 | — |
| | **$Ta_2C$** | — | -1.87 | -2.37 | -2.37 | — |
| $d^4$ | **$Cr_2C$** | — | +0.63 | — | — | — |
| | **$Mo_2C$** | — | -1.61 | — | -1.63 | -1.47 |
| | **$W_2C$** | -1.31 | -1.13 | — | — | — |

Due to the noteworthy $CO_2$ attachment and activation on carbide MXene (0001) surfaces, it is worth investigating the range of temperatures at which the MXenes would capture and store $CO_2$. To this end, transition state theory (TST)[36] based methodology is used to estimate adsorption and desorption rates ($r_{ads}$ and $r_{des}$) over a temperature range up to 2500 K, well below the melting points of parent TMCs, ranging 2900-4200 K.[37] Details on TST models are found in ESI.† Briefly, the adsorption rate depends on the incidence of $CO_2$ to the surface and so on the $CO_2$ partial pressure ($p_{CO2}$). Three different $p_{CO2}$ conditions are evaluated to calculate $r_{ads}$: (*i*) atmospheric $CO_2$ partial pressure, $p_{CO2}$ = 40 Pa,[38] (*ii*) for $p_{CO2}$ = 15000 Pa (or 0.15 bar),[39] a benchmark value for postcombustion exhaust gases, and (*iii*) $p_{CO2} = 10^5$ Pa (or 1 bar), a partial pressure regime of interest for pure $CO_2$ stream generation from a CCS system.[40]

The desorption rates largely depend on the adsorption strenght, and this depends as well on the adsorption conformation (see Table 1). Two desorption fringe situations are considered gaining two temperature-dependent desorption curves for each MXene, either using the weakest $E_{ads}$ value as obtained by PBE and the strongest $E_{ads}$ as obtained by PBE-D3. This choice comprises the least and most favourable adsorption situations, without being biased by the computational accuracy. The estimated $r_{ads}$ and $r_{des}$ are illustrated for extreme situations of $W_2C$ and $Ti_2C$, with lowest and highest $E_{ads}$ values, respectively (see Fig. 2a, Table 1 and Table S1 in ESI†).

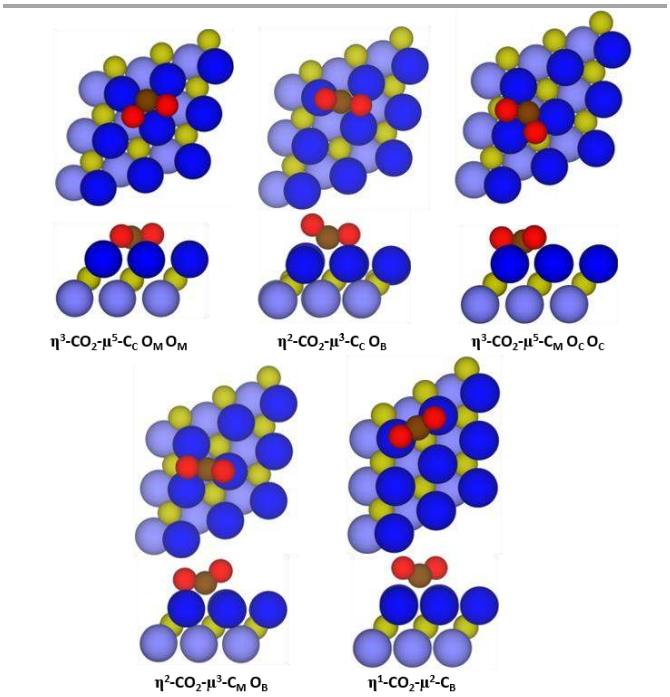


**Fig.1** Side and top views of $CO_2$ adsorbed on $\eta^3$-$CO_2$-$\mu^5$-$C_CO_MO_M$, $\eta^2$-$CO_2$-$\mu^3$-$C_CO_B$, $\eta^3$-$CO_2$-$\mu^5$-$C_MO_CO_C$, $\eta^2$-$CO_2$-$\mu^3$-$C_MO_B$, and $\eta^1$-$CO_2$-$\mu^2$-$C_B$ sites of MXene (0001) surfaces. Carbon and oxygen atoms of the $CO_2$ molecule are represented by brown and red spheres, respectively. MXene (0001) surface is defined with dark and light blue spheres for M upper and bottom layers, respectively, whereas inner carbon layer is represented by dark yellow spheres. Further structural details are found in ESI.†

In Fig. 2a that crossing points between $r_{ads}$ and $r_{des}$ define temperatures below which adsorption prevails and, consequently, $CO_2$ becomes stored. Thus, for $W_2C$ at 40 Pa $p_{CO2}$ (labeled air), the intersection temperature $T_1$ is 344 K for weakest PBE $E_{ads}$, and 696 K ($T_2$) for strongest PBE-D3 $E_{ads}$. $T_1$-$T_2$ defines a temperature range below which $CO_2$ would certainly be stored, and above which it would be certainly desorbed. Note that an increase of $p_{CO2}$ to $15{\cdot}10^3$ Pa shifts these limits $T_3$-$T_4$ to higher, even further at 1 bar pressure in the $T_5$-$T_6$ limit. These three intervals imply temperature ranges where the initial capture and accumulation of $CO_2$ is lost when the system is annealed. The average swich temperature for the set of MXene surfaces is ~ 1250 K (see Fig. 2b), well below that the melting points of parent TMCs, ranging 2900-4200.[37]

Considering this interpretation, the analysis of the rest of MXenes is summarized in Fig. 2b. Note that here only temperature ranges are shown, independent of the particular adsorption site and strength; a further detailed description is reported in Table S2 of the ESI.† From Fig. 2b one notices that consistently those MXene (0001) surfaces with high adsorption energies feature elevated temperature ranges. Therefore, $d^2$ MXenes ($Ti_2C$, $Zr_2C$, $Hf_2C$) show the largest temperature ranges, whereas $d^4$ MXenes feature the smallest. Notice in passing by that $Cr_2C$ was excluded from rate analysis as features (unfavourable) positive $E_{ads}$, see Table 1. For practical purposes, $Mo_2C$ and $W_2C$ are among the most appealing MXenes in case of $CO_2$ capture and posterior release processes.

Last, surface exposure and possible $CO_2$ loading is considered. One main appealing feature of 2D MXene materials is their high surface area. Considering our models dimensions (see ESI†), four molecules of $CO_2$ could be conserbvatively and simultaneously adsorbed on each MXene material surface. For such an idealized situation, one could quantify the amount of $CO_2$ adsorbed per amount of MXene. Present estimations indicate that carbide MXenes can adsorb 2.34–8.25 mol $CO_2$/kg. of substrate, see Fig. 3 and Table S3 of the ESI†. This range clearly shows the high potential of MXene materials for $CO_2$ storage being comparable or even better than zeolites, *e.g.* Ca-X[41] and I3X[42] with 3.36 and 3.96 mol $CO_2$/kg, respectively, or derivates of graphene, *e.g.* a-RGO-950[43] with 3.36 mol $CO_2$/kg, which are clearly better than using bulk MgO nanopowders, with 0.92 mol $CO_2$/kg.[44] In practical operation conditions one should separate $CO_2$ from other competing (combustion) gases prior to adsorption, although recent studies on a series of Mxenes show a high adsoprtion preference for $CO_2$ with respect other gases such as CO or $CH_4$ by more than 1.5 eV.[45]

In summary, $CO_2$ storage on carbide $M_2C$ MXenes (M = Ti, Zr, Hf, V, Nb, Ta, Mo, W) (0001) surfaces is reported by using the state-of-art DFT PBE calculations including D3 Grimme correction dispersion. Results show high adsorption energies up to -3.69 eV accompanied by a $CO_2$ activation, translated into anionic $CO_2^{\delta-}$ species with elongated $\delta$(CO) bonds, bent structures, and a MXene→$CO_2$ charge transfer, unprecedentedly above 2 *e* for $Hf_2C$. Given these high adsorption energies, $M_2C$ MXenes are predicted to be more effective than their 3D bulk counterparts for $CO_2$ capture, storage and activation. Adsorption and desorption rates predicted

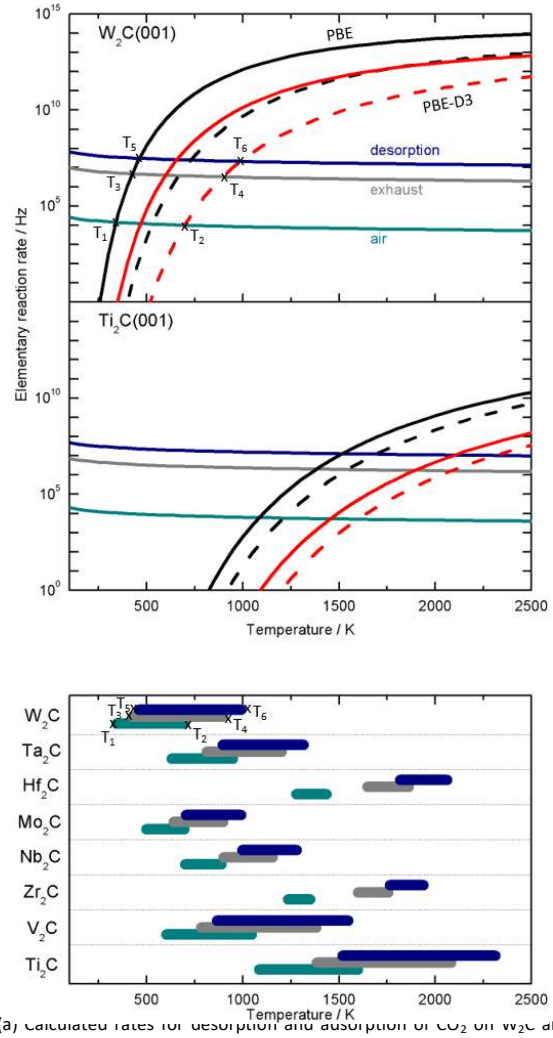


**Fig. 2** (a) Calculated rates for desorption and adsorption of $CO_2$ on $W_2C$ and $Ti_2C$ (0001) surfaces. On $W_2C$ marked points with $T_1$–$T_6$ labels in (a) and (b) show how desorption temperature ranges in (b) have been obtained. Legend for (a): green, gray, and blue colors correspond to adsorption rates on a single site per time unit for a $CO_2$ partial pressures of 40, $15{\cdot}10^3$, and $10^5$ Pa, respectively. Black and red lines are desorption rates per site for PBE (solid) and PBE-D3 (dashed). Legend for (b): green, gray, and blue bars belong to desorption temperatures ranges for $CO_2$ partial pressures of 40, $15{\cdot}10^3$, and $10^5$ Pa, respectively.

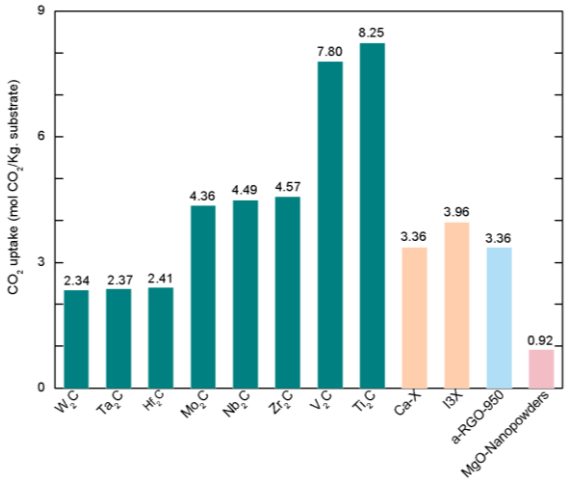


**Fig. 3** Comparison of $CO_2$ uptake in MXene materials with zeolites (Ca-X and I3X), derivates of graphene (a-RGO-950) and bulk MgO nanopowders depicted by green, orange, blue and pink bars, respectively. Further details are found in Table S3 of the ESI.†

from TST models show that these materials can theoretically adsorb $CO_2$ up to elevated temperatures and low partial pressures. Additionally, MXenes can yield $CO_2$ uptakes ranging 2.34–8.25 mol $CO_2$/kg of substrate, quite competitive to other nowadays-existent material solutions. Thus, 2D carbide $M_2C$ MXenes are introduced as potential materials for $CO_2$ capture, where its activated adsorption is further appealing for using them as catalysts on $CO_2$ conversion.

This work has been funded by Spanish *Ministerio de Economía y Competitividad* (MEC) CTQ2015-64618-R grant, partly by *Generalitat de Catalunya* grants 2014SGR97 and XRQTC, and the NOMAD Center of Excellence project, which received funding from the European Union's Horizon 2020 research and innovation programme under Grant Agreement No. 676580. A. M. G. and F. V. thank the Spanish *Ministerio de Economía y Competitividad* for the *Juan de la Cierva* (FJCI-2015-23760) and the *Ramón y Cajal* (RYC-2012-10129) postdoctoral grants, respectively. F. I. acknowledges additional support from the 2015 ICREA Academia Award for Excellence in University Research.

## Notes and references

1 Intergovernmental Panel on Climate Change, *Climate Change 2014*: *Synthesis Report*. IPCC, 1st edn, 2015.

2 V. Balzani, A. Credi and M. Venturi, *ChemSusChem*, 2008, **1**, 26.

3 J. O. Lewis, S. N. Hógáin and A. Borghi, *Building Energy Efficiency in European Cities*. 2013.

4 P. A. Owusu and S. Asumadu-Sarkodie, *Cogent Engineering*, 2016, **3**, 1167990.

5 D. Y. C. Leung, G. Caramanna and M. M. Maroto-Valer, *Renew. Sust. Energ. Rev.*, 2014, **39**, 426.

6 K. P. Kuhl, E. R. Cave, D. N. Abram and T. F. Jamarillo, *Energ. Environ. Sci.*, 2012, **5**, 7050.

7 C. W. Li and M. W. Kanan, *J. Am. Chem. Soc.*, 2012, **134**, 7231.

8 M. Favaro, H. Xiao, T. Cheng, W. A. Goddard III, J. Yano and E. J. Crumlin, *Proc. Natl. Acad. Sci. USA*, 2017, **114**, 6706.

9 J. Wei, Q. Ge, R. Yao, Z. Wen, C. Fang, L. Guo, H. Xu and J. Sun, *Nat. Commun.*, 2017, **8**, 15174.

10 F. Viñes, A. Borodin, O. Höfft, V. Kempter and F. Illas, *Phys. Chem. Chem. Phys.*, 2005, **7**, 3866.

1 1 H. J. Freund and M. W. Roberts, *Surf. Sci. Rep.*, 1996, **25**, 225.

12 S. Posada-Pérez, P. J. Ramírez, J. Evans, F. Viñes, P. Liu, F. Illas and J. A. Rodríguez, *J. Am. Chem. Soc.*, 2016, **138**, 8269.

13 V. A. de la Peña O´Shea, S. González, F. Illas and J. L. G. Fierro, *Chem. Phys. Lett.*, 2008, **454**, 262.

14 D. C. Sorescu, J. Lee, W. A. Al-Saidi and K. D. Jordan, *J. Chem. Phys.*, 2005, **109**, 104707.

15 Y. Jiao, A. Du, Z. Zhu, V. Rudolph, G. Q. Lu and S. C. Smith, *Catal. Today*, 2011, **175**, 271.

16 D. Smykowski, B. Szyja and J. Szczygiel, *J. Mol. Graphics Modell.*, 2013, **41**, 89.

17 C. A. Trickett, A. Helal, B. A. Al-Maythalony, Z. H. Yamani, K. E. Cordova and O. M. Yaghi, *Nat. Rev. Mater.*,2017, **2**, 17045.

18 Y. Xiao, J.-Y. Hwang and Y.-K. Sun, *J. Mater. Chem. A*, 2016, **4**, 10379.

19 C. Kunkel, F. Viñes and F. Illas, *Energy Environ. Sci.*, 2016, **9**, 141.

20 F. Viñes, C. Sousa, P. Liu, J. A. Rodriguez and F. Illas, *J. Chem. Phys.*, 2005, 122, 174709.

21 X. Liu, C. Kunkel, P. Ramírez de la Piscina, N. Homs, F. Viñes, and F. Illas, *ACS Catal.*, 2017, **7**, 4323.

22 C. Giordano, C. Erpen, W. Yao, B. Milke and M. Antonietti, *Chem. Mater.*, 2009, **32**, 5136.

23 M. Naguib, O. Mashtalir, J. Carle, V. Presser, J. Lu, L. Hultman, Y. Gogotsi and M. W. Barsoum, *ACS Nano*, 2012, **6**, 1322.

24 B. Anasori, M. R. Lukatskaya and Y. Gogotsi, *Nat. Rev. Mater.*, 2017, **2**, 16098.

25 X. Yu, X. Cai, H. Cui, S.-W. Lee, X.-F. Yu, B. Liu, *Nanoscale*, 2017, **9**, 17859.

26 Y. Xie, M. Naguib, V. N. Mochalin, M. W. Barsoum, Y. Gogotsi, X. Yu, K. W. Nam, X. Q. Yang, A. I. Kolesnikov and P. R. C. Kent, *J. Am. Chem. Soc.*, 2014, **136**, 6385.

27 D. Er, J. Li, M. Naguib, Y. Gogotsi and V. B. Shenoy, *ACS Appl. Mater. Interfaces*, 2014, **6**, 11173.

28 W. F. Chen, C. H. Wang, K. Sasaki, N. Marinkovis, W. Xu, J. T. Muckerman, T. Zhu and R. R. Adzic, *Energy Environ. Sci.*, 2013, **6**, 943.

29 A. Vojvodic, C. Ruberto and B. I. Lundqvist, *J. Phys.: Condens. Matter*, 2010, **22**, 375504.

30 J. P. Perdew, K. Burke and M. Ernzerhof, *Phys. Rev. Lett.*, 1996, **77**, 3865.

31 G. Kresse and J. Furthmüller, *Phys. Rev. B: Condens. Matter Mater. Phys.*, 1996, **54**, 11169.

32 S. Grimme, S. Ehrlich and L. Goerigk, *J. Comput. Chem.*, 2011, **32**, 1456.

33 S. Posada-Pérez, F. Viñes, P. J. Ramírez, A. B. Vidal, J. A. Rodriguez and F. Illas, *Phys. Chem. Chem. Phys.*, 2014, **16**, 14912.

34 L. M. Azofra, N. Li, D. R. MacFarlane and C. Sun, *Energy Environ. Sci.*, 2016, **9**, 2545.

35 R. F. W. Bader, *Acc. Chem. Res.*, 1985, **18**, 9.

36 K. Reuter, in *Modelling and Simulation of Heterogeneous Catalytic Reactions*, Wiley-VCH Verlag GmbH & Co. KGaA, 2011, ch. 3.

37 L. E. Toth, *Transition Metal Carbides and Nitrides*, Academic Press: New York, 1971.

38 T. Takahashi, S. Sutherland and A. Kozyr, *Global Ocean Surface Water Partial Pressure of $CO_2$ Database: Measurements Performed During 1957-2014 (Version 2014)*, Environmental Sciences Division. Oak Ridge National Laboratory, 2015.

39 D. M. D´Alessandro, B. Smit and J. R. Long, *Angew. Chem. Int. Ed.*, 2010, **49**, 6058.

40 M. E. Boot-Handford, J. C. Abanades, E. J. Anthony, M. J. Blunt, S. Brandani, N. Mac Dowell, J. R. Fernández, M.-C. Ferrari, R. Gross, J. P. Hallett, R. S. Hazseldine, P. Heptostall, A. Lyngfelt, Z. Makuch, E. Mangano, R. T. J. Porter, M. Pourkashanian, G. T. Rochelle, N. Shah, J. G. Yao and P. S. Fennell, *Energy Environ. Sci.*, 2014, **7**, 130.

41 T.-H. Bae, M. R. Hudson, J. A. Mason, W. L. Queen, J. J. Dutton, K. Sumida, K. J. Micklash, S. S. Kaye, C. M. Brown and J. R. Long, *Energy Environ. Sci.*, 2013, **6**, 128.

42 C. Chen, D.-W. Park and W.-S. Ahn, *Appl. Surf. Sci.*, 2014, **292**, 63.

43 S. Chowdhury and R. Balasubramanian, *Ind. Eng. Chem. Res.*, 2016, **55**, 7906.

44 W. Gao, T. Zhou, B. Louis, Q. Wang, *Catalysts* 2017, **7**, 116.

45 N.Li, X. Chen, W.-J. Ong, D. R. MacFarlane, X. Zhao, A. K. Cheetham, C. Sun, *ACS Nano* 2017, **11**, 10825.